

Dalton Transactions

An international journal of inorganic chemistry

Accepted Manuscript

This article can be cited before page numbers have been issued, to do this please use: T. Das, D. Singha and M. Nandi, *Dalton Trans.*, 2020, DOI: 10.1039/D0DT01922D.



This is an Accepted Manuscript, which has been through the Royal Society of Chemistry peer review process and has been accepted for publication.

Accepted Manuscripts are published online shortly after acceptance, before technical editing, formatting and proof reading. Using this free service, authors can make their results available to the community, in citable form, before we publish the edited article. We will replace this Accepted Manuscript with the edited and formatted Advance Article as soon as it is available.

You can find more information about Accepted Manuscripts in the [Information for Authors](#).

Please note that technical editing may introduce minor changes to the text and/or graphics, which may alter content. The journal's standard [Terms & Conditions](#) and the [Ethical guidelines](#) still apply. In no event shall the Royal Society of Chemistry be held responsible for any errors or omissions in this Accepted Manuscript or any consequences arising from the use of any information it contains.

Big effect of a small change: formation of CuO nanoparticles instead of covalently bound Cu(II) over functionalized mesoporous silica and its impact on catalytic efficiency

Trisha Das, Debdas Singha and Mahasweta Nandi*

*Integrated Science Education and Research Centre, Siksha Bhavana, Visva-Bharati University, Santiniketan 731
235, India*

Email: mahasweta.nandi@visva-bharati.ac.in

Abstract

Two different heterogeneous catalysts, one with Cu(II) covalently bonded to functionalized mesoporous silica (**FMS-Cu(II)**) and another with CuO nanoparticles immobilized over the same silica (**FMS-CuO-np**), have been synthesized by a common route but with minor alteration of sequence of addition of the reagents. It is interesting to find that by merely changing the order of addition of reagents Cu(II) can be incorporated into the framework in two different forms. In one case Cu(II) binds to the N and O donor centers present in the functionalized material whereas in other CuO nanoparticles are generated *in situ*. The materials have been thoroughly characterized by powder X-ray diffraction, nitrogen adsorption/desorption, transmission electron microscopy, thermal analysis and FT-IR, solid state MAS-NMR and atomic absorption spectrophotometric studies. The synthesized products have been tested for their catalytic efficiencies in the oxidation of olefins, as a model case. Styrene, α -methyl styrene, cyclohexene, *trans*-stilbene and cyclooctene have been used as substrates in the presence of *tert*-butyl hydroperoxide as the oxidant in acetonitrile medium under mild conditions. The products of the catalytic studies have been identified and estimated by gas chromatography and gas chromatography-mass spectrometer. The rate of conversion of the substrates for both the catalysts is high and selectivity is also good. But from comparative studies, it is found that **FMS-CuO-np** which contains CuO nanoparticles shows better efficiency over **FMS-Cu(II)**. The catalysts have been recycled for five catalytic cycles without showing much drop in their catalytic activity.

Introduction

Transition metal catalyzed organic transformations have made a position of their own in academia as well as industry because they not only yield valuable products but also make it possible to introduce new functional groups in relatively inert substrates. In this respect, copper based catalysts have been extensively used for various conversions because of their cost-effectiveness and efficiency.^{1,2} These include both homogeneous as well as heterogeneous catalysts, with their respective advantages and disadvantages which have been extensively discussed in the literature.^{3,4} Here the primary focus is on heterogeneous catalysts based on solid support that are easily separable from the reaction medium and can be reused. Different types of solid support *e.g.* polymer,^{5,6} zeolite,⁷ silica,⁸ graphene,⁹ mesoporous carbon,¹⁰ metal-organic framework,¹¹ metal oxide nanoparticles,¹² *etc.*^{13,14} are known. Among these, mesoporous silica is distinctly different and has been frequently employed because it allows better interaction between the metal center and the substrate due to its large surface area¹⁵ which significantly improves the efficiency of the catalysts. Silica framework is thermally and chemically stable and functionalization can be carried out easily to introduce organic components with various donor atoms like N, O or S. These heteroatoms can either bind a metal ion to the porous framework through covalent interaction¹⁶ or stabilize metal based nanoparticles over the solid support by non-covalent interactions.¹⁷ In any case, the functionalization of silica support is so adjusted that it binds/stabilizes the metal ion strongly and does not allow it to dissociate during the catalytic process in solution. Though there have been numerous works on mesoporous silica based effective catalysts, very few reports have focused on the synthesis aspect of such catalysts. As mentioned before, silica frameworks offer the advantage of flexibility of functionalization which leads to a host of possibilities. Thus, it is indeed interesting to explore how a small variation in the methodology can bring about major change in the structure of the materials and how that change can affect their efficiency as catalysts.

Though there are relatively few studies, so far, discussing how small reaction parameters can be responsible in bringing about significant changes in the structure of the resulting hybrid material, such paradigms do exist. It has been found that merely the sequence of addition of reagents can significantly influence the size distribution of gold nanoparticles¹⁸ or the mixing time between the precursor and the ligand can become a key parameter in controlling the size and shape of ZnO nanoparticle and the processable hybrid materials.¹⁹ The synthesis route is also found to have important structural effects on NiO_x nanoparticles that can enhance their electrocatalytic oxidation property.²⁰ Sometimes the addition rate of the precursor to a stock solution can also play an important role in the control of nanocrystal structures by triggering some unexpected side reaction.²¹ For mesoporous silica supported structures, the mesopore dimension²² or the anion of the metal salt used²³ can also have pronounced effect on the catalytic properties. It is established that nanoparticle based structures show physical and chemical properties that are distinctly different from their bulk counter-parts.²⁴ This is primarily because of their increased surface to volume ratio with respect to the material in the bulk form and catalysis is all about the surface. Investigations on the catalytic activity of metal nanoparticles and bulk materials have revealed

the better efficiency of the nano-systems.²⁵ Nanostructured metal based catalysts have shown their potential utility and played crucial role in various organic syntheses and methodologies²⁶⁻²⁸ and the effectiveness of CuO nanoparticle-based catalysts has been explored in this regard.²⁹⁻³¹

In this article, it has been shown how the sequence of addition of reactants can be important and playing with it a little can give rise to two completely different structures. Here two different materials, **FMS-Cu(II)** and **FMS-CuO-np**, with distinctly different features, have been obtained from a common SBA-15 functionalized silica support. The starting functionalized silica which is used in both the cases has been obtained by the reaction of mesoporous SBA-15 with 3-aminopropyl triethoxy silane (3-APTES) followed by *tris*(4-formyl phenyl)amine (Scheme 1). For **FMS-Cu(II)**, the subsequent synthesis has been carried out in two-steps: first 2-aminophenol is allowed to react with the functionalized silica and then the product is treated with CuCl₂.2H₂O to incorporate Cu(II) into the framework through covalent interaction with N and O donor centers. On the other hand, for **FMS-CuO-np**, 2-aminophenol and CuCl₂.2H₂O have been allowed to react together with the functionalized silica in one step to generate CuO nanoparticles instead, which are stabilized through non-covalent interactions. This change in the form of the metal center, brings about significant change in the catalytic properties of **FMS-Cu(II)** and **FMS-CuO-np**. The latter with better surface exposure of CuO nanoparticles shows higher catalytic activity and is superior over the Cu(II)-coordinated material, and gives higher yields with better atom economy. To establish this, the materials have been used as catalysts for industrially significant alkene oxidation reaction with wide applicability, as a model case. The reactions have been carried over styrene, α -methyl styrene, cyclohexene, *trans*-stilbene and cyclooctene substrates in the presence of *tert*-butyl hydroperoxide (TBHP) as the oxidant under mild conditions.

Among the various transition metal catalyzed reactions like polymerization,³² C–N bond activation,³³ oxidation of alkanes and alkenes,^{34,35} alcohol oxidation,³⁶ C–C bond formation,³⁷ hydrogenation,³⁸ *etc.*,³⁹⁻⁴¹ oxidation of alkenes is by far one of the most important. Large quantities of feed-stocks for this reaction are available in nature in the form of fuel and gases.⁴² Apart from that, various valuable chemical products like drug intermediates,⁴³ food additives and agrochemicals^{44,45} can be obtained from alkene oxidation reactions. Alkene oxidation is generally accomplished with hydrogen peroxide, *tert*-butyl hydroperoxide, iodosyl benzene, molecular oxygen, *etc.* as oxidant to get the corresponding epoxide as the major product with other parallel products, in the presence of a suitable catalyst.⁴⁶ Epoxides are important building units in the synthesis of several organic fine chemicals and molecules of biological importance, and epoxidation reactions can introduce two chiral carbon centers in a molecule.^{47,48} Thus, keeping in mind the broader perspective of olefin oxidation reactions it has been chosen as a typical example in this study.

Experimental Section

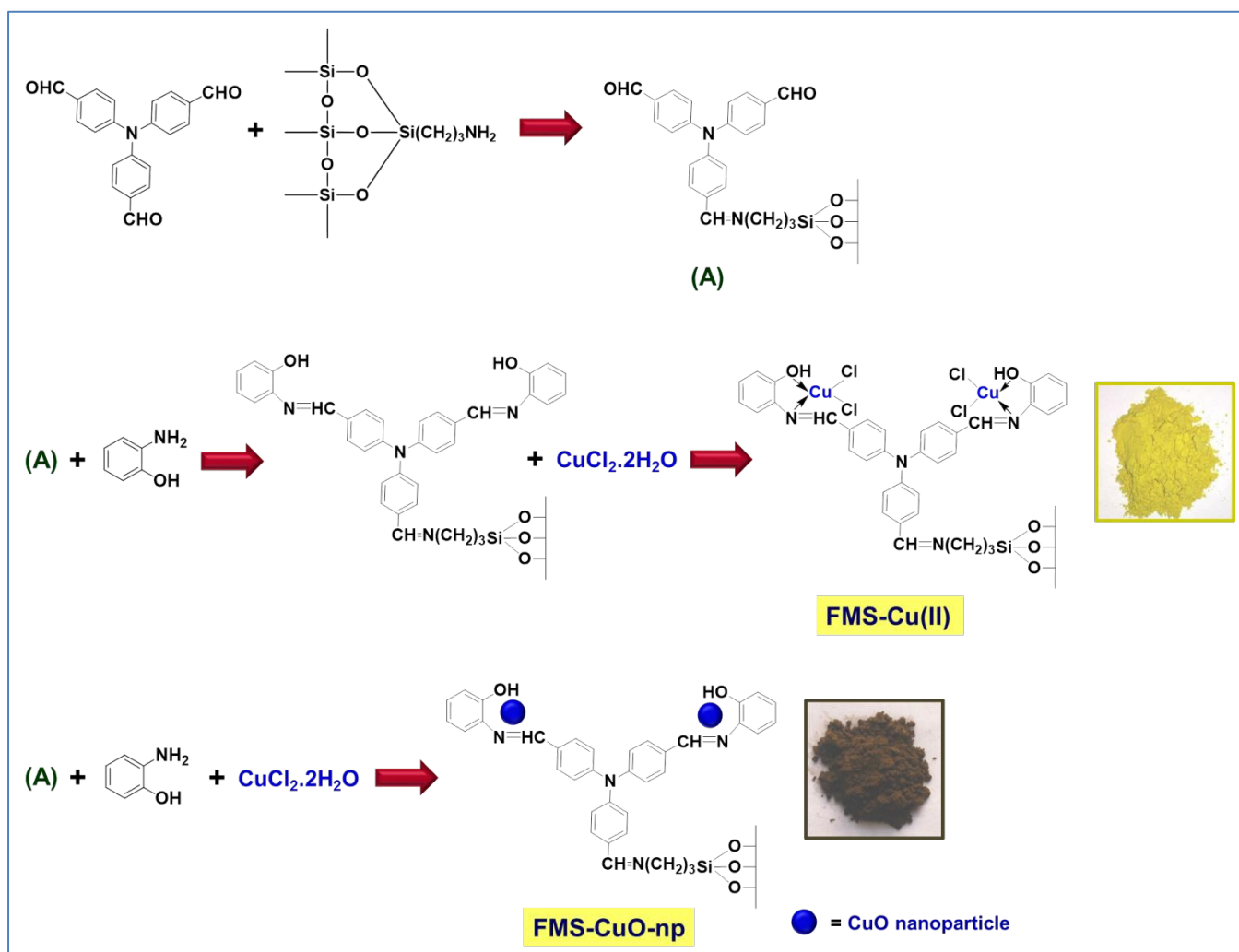
Materials and physical measurements

Tetraethyl orthosilane (TEOS), 3-aminopropyltriethoxysilane (3-APTES), Pluronic P123 (a poly(ethylene glycol)-block-poly(propylene glycol)-block-poly(ethylene glycol) block copolymer), triphenylamine, phosphorus oxychloride (POCl_3), styrene, α -methyl styrene, cyclohexene, *trans*-stilbene, cyclooctene and *tert*-butyl hydroperoxide (TBHP) have been purchased from Sigma-Aldrich. Hydrochloric acid (HCl) and cupric chloride dihydrate ($\text{CuCl}_2 \cdot 2\text{H}_2\text{O}$) have been procured from E-Merck and 2-aminothiophenol from TCI. Other solvents used in the synthesis are purchased from commercial sources and used without further purification. Low and high angle powder X-ray diffraction patterns of the samples have been recorded on a Bruker D-8 Advance diffractometer using Ni-filtered Cu- $K\alpha$ radiation ($\lambda = 1.5406 \text{ \AA}$) at 40 kV and 40 mA. Nitrogen adsorption-desorption isotherms of the samples are recorded at 77 K using a NOVA 2200e, Quantachrome Instruments, Surface Area and Pore Size Analyzer. The samples are degassed for 8-12 h at 343, 363, 393 or 423 K depending on their nature before performing the measurements and the specific surface areas are estimated using Brunauer-Emmett-Teller (BET) method. For obtaining the pore size distributions, non-local density functional theory (NLDFT) model has been used. The transmission electron microscopic (TEM) images are recorded in a JEOL JEM-1400 transmission electron microscope. Sample preparations have been done by putting one drop of the samples dispersed in ethanol on a thin layer of amorphous carbon coated copper grid (400 mesh). All FT-IR spectra of the samples have been measured on a Spectrum Two, Perkin Elmer spectrometer using attenuated total reflectance (ATR) method. Thermogravimetric analyses (TGA) have been carried out under nitrogen atmosphere (flow rate: 50 cc/min) from 298 K to 1073 K (at heating rate of 2 K/min) using a Perkin Elmer STA-6000 thermal analyzer. Solid state MAS NMR analyses are performed in a CHEMAGNETICS 300 MHz CMX 300 spectrometer. To determine the content of Cu present in **FMS-Cu(II)** and **FMS-CuO-np**, atomic absorption spectrophotometric (AAS) studies have been carried out using a Perkin Elmer PinAAcle 900F atomic absorption spectrometer. To prepare the sample solutions, 0.04 g of the catalysts have been dispersed in 2 ml of DTPA (diethylenetriaminepentaacetic acid) solution and the volumes are made up to 20 ml by adding distilled water. Then the solutions have been shaken for 2 hours and membrane filtered. The obtained colorless filtrates have been used for the analysis. The substrates and products formed in the catalytic reactions are analyzed by using a next generation high speed gas chromatography (GC) system, Shimadzu GC-2025 AF, equipped with a fused silica capillary column and a FID detector. Substrate and products have been identified by PerkinElmer Clarus 680/600 T Gas Chromatography-Mass Spectrometer (GC-MS).

Preparation of the materials, **FMS-Cu(II)** and **FMS-CuO-np**

The mesoporous silica support chosen for the syntheses here is SBA-15. A typical synthesis of SBA-15 is carried out by first adding 1.7 g of Pluronic P123 to 62 ml of water taken in a polypropylene bottle. The mixture is kept

under continuous stirring until a clear solution is obtained. Then 6.0 g of 35% HCl is added to this solution followed by the drop wise addition of 3.5 g of TEOS as the silica source after some time. Then the mixture is stirred for 20 h at 313 K. The resulting white gel is transferred into an autoclave and heated at 373 K for 20 h without stirring. Then the autoclave is cooled to room temperature, the product is filtered and washed with water followed by ethanol for two-three times each. After that the white colored residue is dried and then calcined at 773 K for 10 h in a flow of air. SBA-15 thus synthesized is functionalized with 3-aminopropyl groups by stirring 1.0 g of the mesoporous silica with 1.5 g of 3-APTES overnight in chloroform at room temperature under inert nitrogen atmosphere. The mixture is then filtered and the product is washed repeatedly, first with chloroform and then dichloromethane. Finally, the $-\text{NH}_2$ functionalized SBA-15 is obtained after drying the residue in air.



Scheme 1: Synthesis of FMS-Cu(II) and FMS-CuO-np

Tris(4-formyl phenyl)amine, a trialdehyde, is synthesized *via* Vilsmeier-Haack formylation reaction of triphenylamine and phosphorus oxychloride following a method reported previously.⁴⁹ This trialdehyde is attached to the 3-APTES functionalized SBA-15 by the reaction of one of its aldehyde group with the -NH_2 group of the 3-aminopropyl moiety (Scheme 1). For that, the 3-APTES functionalized silica is refluxed with *tris*(4-formyl phenyl)amine for 4 h in methanolic medium. The molar ratio is kept such that two -CHO groups of the trialdehyde remain free for further functionalization. The resulting light yellow colored product (**A**) is separated by filtration, washed several times with methanol until the filtrate becomes colorless.

Both **FMS-Cu(II)** and **FMS-CuO-np** have been synthesized from this trialdehyde grafted mesoporous SBA-15 (**A**). For the synthesis of **FMS-Cu(II)** (Scheme 1), **A** is refluxed with 2-aminophenol in 1:2 molar ratio so as to react the two residual -CHO groups of the trialdehyde to the two -NH_2 groups of aminophenol by Schiff base condensation.⁵⁰ The reaction is carried out for 4 h in methanol medium and the dark yellow solid product is recovered by filtration followed by washing thoroughly with methanol. Then this product is refluxed with $\text{CuCl}_2 \cdot 2\text{H}_2\text{O}$ (taken in equivalent amount with respect to the -NH_2 groups coming from 2-aminophenol) for 4 h in acetonitrile medium to obtain a yellowish-green residue. This residue is separated by filtration, washed thoroughly with acetonitrile to ensure complete removal of the unreacted salt and dried in vacuum to get the final product.

On the other hand, synthesis of **FMS-CuO-np** is carried out in single step, unlike the previous synthesis which has been carried out in two steps.¹⁷ In this case, **A**, 2-aminophenol and $\text{CuCl}_2 \cdot 2\text{H}_2\text{O}$ are taken in methanol in a round bottom flask in 1:2:2 molar ratio and the mixture is refluxed for 4 h (Scheme 1). In this case the residue is found to be brown in color which is isolated by filtration and washed with methanol until all the unreacted substances are removed. The product after drying gives the desired material.

Oxidation of Olefins

Liquid phase oxidation reactions of olefins, namely, styrene, α -methyl styrene, cyclohexene, *trans*-stilbene and cyclooctene, are carried out using **FMS-Cu(II)** and **FMS-CuO-np** as the catalysts in presence of *tert*-butyl hydroperoxide (TBHP) as the terminal oxidant in acetonitrile medium under mild conditions. The heterogeneous oxidation reactions are performed in a two-necked round-bottomed flask fitted with a condenser and placed in a temperature controlled oil bath under rapid stirring. Typically, 1 mmol of the substrate is added to 5 ml of acetonitrile followed by the addition of 10 mg of the catalyst (**FMS-Cu(II)**/**FMS-CuO-np**) and the mixture is preheated to 338 K. The reaction is initiated with the addition of *tert*-butyl hydroperoxide (equimolar with respect to the substrate). Aliquots from the reaction mixture are collected at regular intervals, cooled and nitrobenzene is added as the internal standard. The substrate and product(s) from the reaction mixture are analyzed by gas chromatography and identified by comparison with known standards/GC-MS. A blank reaction has also been carried out for each substrate without adding any catalyst and keeping other experimental conditions unchanged.

To check recyclability, the catalysts are recovered by filtration and washed thoroughly with acetonitrile. The residues are then treated with 0.1 M HCl solution in ethanol for 8 h at 343 K and dried at 373 K for 2 h. The catalytic reactions are again carried out with the recovered catalysts following the same experimental procedure. Apart from this, for optimization of temperature, the reactions have been carried out at different temperature (ambient, 318 K, 328 K and 348 K). Additionally, the reactions have been carried out in the presence of hydrogen peroxide and molecular oxygen as prospective oxidizing agents.

Results and discussion

Synthesis

The materials, **FMS-Cu(II)** and **FMS-CuO-np** have been synthesized following the synthetic route depicted in Scheme 1. Synthesis of both the materials involves the common trialdehyde functionalized mesoporous silica, **A**. However, it is interesting to note that when the synthesis is carried out in two steps, first to introduce N and O donor atoms in the mesoporous silica framework by incorporating 2-aminophenol by Schiff base condensation with the two residual -CHO groups of the trialdehyde followed by the reaction with $\text{CuCl}_2 \cdot 2\text{H}_2\text{O}$, Cu(II) gets covalently bound to the silica framework. This gives **FMS-Cu(II)**. On the other hand, when the reaction is carried out in a single step by mixing all the reactants (*i.e.* **A**, 2-aminophenol and $\text{CuCl}_2 \cdot 2\text{H}_2\text{O}$) together, CuO nanoparticles are formed *in situ* in the reaction medium and get uniformly distributed over the mesoporous silica support. This generates **FMS-CuO-np**. The difference between the two materials can also be witnessed from their color; while the former is yellowish-green in color due to the formation of coordinated Cu(II) the latter is brown in color due to the generation of CuO nanoparticles.

Preparation of **FMS-Cu(II)** takes place following the conventional route, where the 2-aminophenol molecules first bind the functionalized silica through Schiff-base reaction with the two residual -CHO groups. After this, any unreacted 2-aminophenol is removed from the product by repeated washing with methanol. Then it is refluxed with $\text{CuCl}_2 \cdot 2\text{H}_2\text{O}$ taken in acetonitrile solvent when Cu(II)-binds to the N and O donor atoms of the functionalized silica.⁵⁰ On the other hand, in the preparation of **FMS-CuO-np**, 2-aminophenol and $\text{CuCl}_2 \cdot 2\text{H}_2\text{O}$ are both taken together in methanol under refluxing condition which generates nanoparticles of CuO. Synthesis of nanoparticles still remains largely empirical; though several facts can be explicated a posteriori, it is almost impossible to envisage the outcome of a reaction which involves new reactants.²¹ Sometimes, specific unpredicted aspects inherent in a particular reaction can become the governing factor over the general principles. In this case, probably 2-aminophenol acts as a ligand that can stabilize the nanoparticles and control the precise molecular definition of the material³ when they are formed *in situ* in the reaction mixture under elevated temperature in methanolic medium.¹⁷ The 2-aminophenol units which stabilize the CuO nanoparticles simultaneously bound to the functionalized silica through Schiff-base reaction and immobilize the nanoparticles homogeneously over the silica support. Thus, Cu(II) is arrested and stabilized in CuO nanoparticle phase instead of covalently bound

Cu(II). In the subsequent section, the distinct structural features of the two materials shall be established by using various characterization tools.

Mesoporosity and microstructure

The diffraction patterns from powder X-ray studies of the samples including **FMS-Cu(II)** and **FMS-CuO-np** are given in Fig. 1. The samples exhibit 2D-ordered hexagonal mesostructure which is evidenced from the appearance of three distinct diffraction peaks corresponding to (100), (110) and (200) planes and a weak signal for (210) plane.⁵¹ With stepwise functionalization of SBA-15 with 3-APTES and then the trialdehyde, the ordering of pores is affected to some extent (Fig. 1a-c). As a result, lowering in peak intensity and shifting of the peaks to higher 2θ values is observed. The latter is attributed to the decrease in pore size of the materials on successive functionalization. However, on formation of **FMS-Cu(II)** and **FMS-CuO-np** from **A**, no significant change in d -spacing takes place (Fig. 1d and e) indicating that the pore sizes are not affected much on incorporation of Cu(II) or CuO nanoparticles, respectively. The wide angle X-ray diffraction patterns of **FMS-Cu(II)** and **FMS-CuO-np** have been shown in Fig. 2. It can be seen that for **FMS-Cu(II)** (Fig. 2a) no diffraction peak arises at higher 2θ values except a wide hump between $15\text{-}30^\circ$ primarily indicating the amorphous nature of the sample. On the other hand, for **FMS-CuO-np** (Fig. 2b) several diffraction peaks can be observed which can be assigned to the characteristic planes of CuO nanoparticles.⁵² The peaks have been indexed and shown in the figure. Thus, it can be concluded that CuO nanoparticles have been formed *in situ* in the material which has been prepared from **A** in a single step.

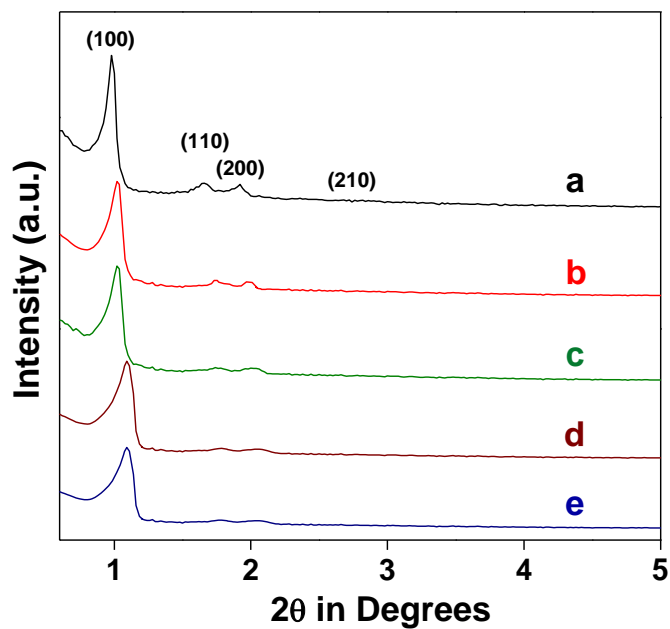


Fig. 1: Small angle powder X-ray diffraction patterns of (a) SBA-15, (b) 3-APTES functionalized SBA-15, (c) trialdehyde functionalized silica (A), (d) **FMS-Cu(II)** and (e) **FMS-CuO-np**.

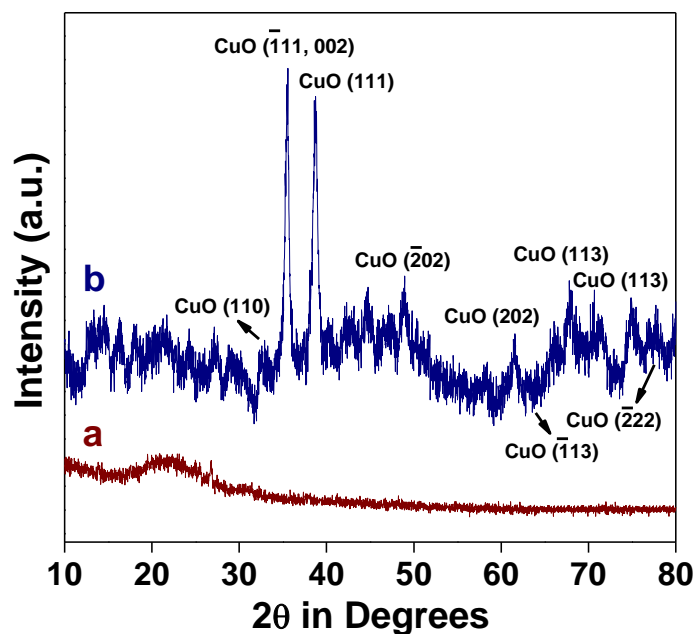


Fig. 2: Wide angle powder X-ray diffraction patterns of (a) **FMS-Cu(II)** and (b) **FMS-CuO-np**.

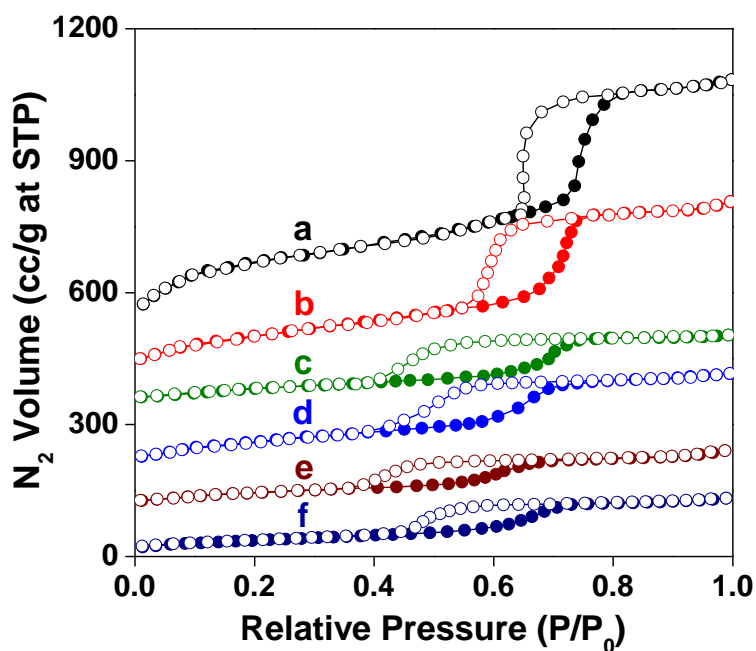


Fig. 3: Nitrogen adsorption/desorption isotherms of (a) SBA-15, (b) 3-APTES functionalized SBA-15, (c) trialdehyde functionalized silica (A), (d) 2-aminophenol functionalized A, (e) **FMS-Cu(II)** and (f) **FMS-CuO-np**. For clarity, Y-axis values have been increased by 460, 385, 300, 190 and 100 cc/g for plot a, b, c, d, and e, respectively. Adsorption points are marked by filled symbols and desorption points by empty symbols.

For porous materials, nitrogen physisorption is an important study to understand the total surface area, pore size and pore volume of the material. Nitrogen adsorption/desorption isotherms have been recorded for the materials at each step of functionalization starting from the mesoporous silica support, SBA-15. From the isotherms plotted in Fig. 3, we get an overall idea about the adsorption/desorption patterns of calcined SBA-15, 3-APTES functionalized SBA-15, trialdehyde functionalized silica (**A**), 2-aminophenol grafted on **A**, **FMS-Cu(II)** and **FMS-CuO-np**. The BET surface area, pore volume and pore size of all the samples have been given in Table 1. Comparing these data, it can be inferred that a gradual decrease in surface area takes place as the starting mesoporous silica is functionalized more and more. This is understandable because with gradual functionalization the surfaces become occupied by various organic and inorganic moieties resulting in the decrease in surface area. The pattern of the isotherms of all the materials is of type IV with a steep rise at higher pressures because of capillary condensation. This indicates the mesoporous nature of the materials.⁵³ Further, the isotherms of all the samples show hysteresis loops defined as type H1 by the IUPAC and is associated to the presence of well-defined cylindrical pore channels⁵⁴ and intercrystallite adsorption.⁵⁵ The average pore diameter of the mesoporous silica support, SBA-15 obtained by non-local density functional theory (NLDFT) model is 8.16 nm (Fig. 4). Pore sizes of the subsequent materials obtained using the same model is found to follow a descending trend *i.e.* with stepwise functionalization in the materials, pore size decreases. Gradual incorporation of functional groups on the pore wall of the silica framework leads to narrowing of the pore opening. This trend is also observed for the pore volume of the samples. The pore volumes of **FMS-Cu(II)** and **FMS-CuO-np** are almost same.

Table 1: Surface area, pore volume and pore size of the starting silica support, intermediates and catalysts

Sl. No.	Sample	BET surface area (m ² /g)	Pore volume (cc/g)	Pore size (nm)
(a)	SBA-15	709	0.965	8.16
(b)	3-APTES functionalized SBA-15	425	0.722	7.29
(c)	Tris(4-formyl phenyl)amine loaded on (b) (A)	239	0.310	5.93
(d)	2-Aminophenol grafted on A	201	0.250	5.01
(e)	FMS-Cu(II)	139	0.210	4.15
(f)	FMS-CuO-np	136	0.205	4.80

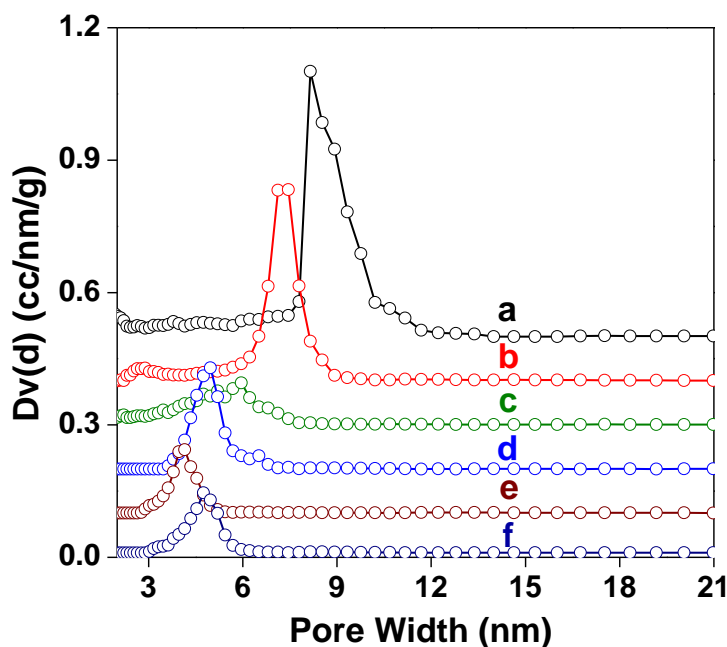


Fig. 4: NLDFT pore size distribution of (a) SBA-15, (b) 3-APTES functionalized SBA-15, (c) trialdehyde functionalized silica (**A**), (d) 2-aminophenol functionalized **A**, (e) **FMS-Cu(II)** and (f) **FMS-CuO-np**. For clarity, Y-axis values have been increased by 0.5, 0.4, 0.3, 0.2 and 0.1 cc/nm/g for plot a, b, c, d and e, respectively.

The transmission electron microscopic (TEM) images of trialdehyde functionalized mesoporous silica (**A**), and the catalysts **FMS-Cu(II)** and **FMS-CuO-np** are shown in Fig. 5. The image for trialdehyde functionalized mesoporous silica, **A** (Fig. 5a) shows well-defined hexagonally arranged mesoporous structure as desirable for an appropriate solid support for the catalysts. When **A** is further functionalized with 2-aminophenol and Cu(II) is bound covalently in the following step to get **FMS-Cu(II)**, the ordering of the pores is decreased to some extent (Fig. 5b) but the hexagonal mesostructure is still retained. The TEM image of **FMS-CuO-np** is shown in Fig. 5c. Spherical nanoparticles of CuO could be seen dispersed over the functionalized mesoporous silica support and having diameter of about 5-7 nm. This indicates the formation of CuO nanoparticles *in situ* when both 2-aminophenol and the Cu(II) salt are allowed to react together with **A**. In this case also the hexagonal arrangement of the pores is retained. Thus, the microstructure and mesoporosity of the functionalized silica as well as the two end products, and formation of CuO nanoparticles can be well elucidated from the low and high angle powder X-ray diffraction patterns, N₂ sorption isotherms and TEM images.

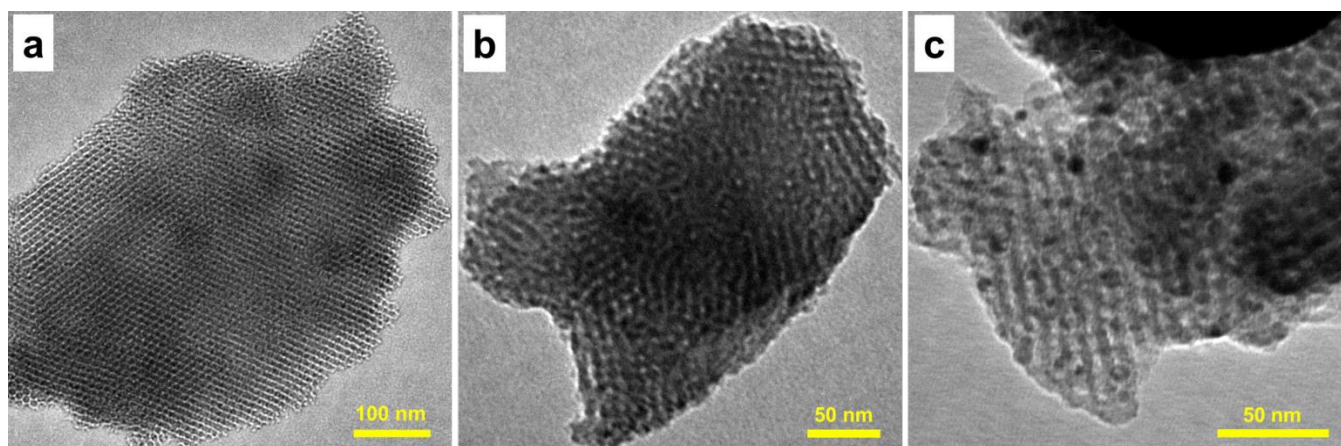


Fig. 5: TEM images of (a) trialdehyde functionalized silica (**A**), (b) **FMS-Cu(II)** and (c) **FMS-CuO-np**.

FT-IR spectra and thermal studies

FT-IR spectra of the materials at various stages have been studied by attenuated total reflectance technique with the powdered samples and shown in Fig. 6. The spectrum of 3-APTES functionalized silica (Fig. 6b) shows a broad band in the region of $3747\text{--}2929\text{ cm}^{-1}$ which may be ascribed to the presence of amino group and methylene moiety in the material. From this it can be inferred that 3-aminopropyl groups has been successfully incorporated in mesoporous silica support where the characteristic band for --NH_2 or --CH_2 groups are absent (Fig. 6a). For the trialdehyde amine grafted silica, **A** (Fig. 6c) two additional peaks arise at around 1702 and 1642 cm^{-1} , which correspond to the presence of azomethine bond (--C=N) and free aldehyde group (--CHO), respectively, in the material. Further, when 2-aminophenol is allowed to react with the free --CHO groups of **A**, a broad band appears in the region of $3022\text{--}3588\text{ cm}^{-1}$ (Fig. 6d) which can be attributed to the free --OH groups of the former. For **FMS-Cu(II)** and **FMS-CuO-np** (Fig. 6e and f) the --C=N stretching frequency is red shifted in both from 1642 cm^{-1} to 1599 cm^{-1} and 1597 cm^{-1} , respectively, which is an indication of retention of the azomethine bond even after interaction with the metal ion.

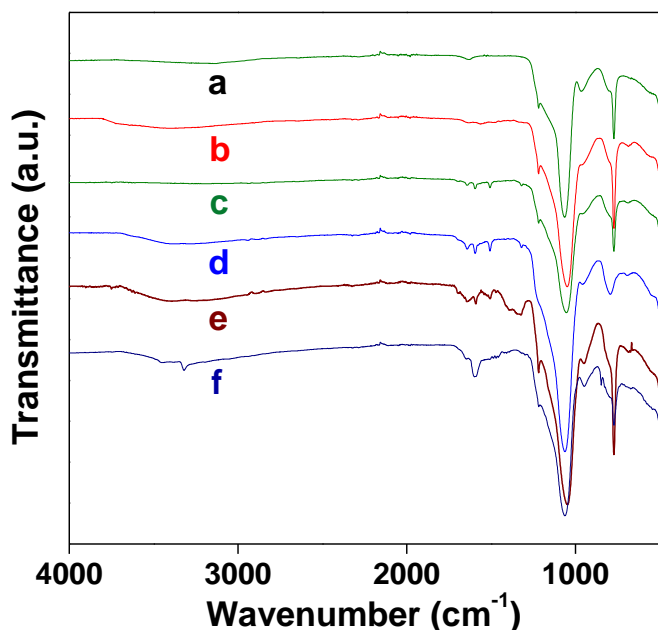


Fig. 6: FT-IR spectra of (a) SBA-15, (b) 3-APTES functionalized SBA-15, (c) trialdehyde functionalized silica (A), (d) 2-aminophenol functionalized A, (e) FMS-Cu(II) and (f) FMS-CuO-np.

Thermogravimetric analyses (TGA) have been carried out for calcined SBA-15, 3-APTES functionalized SBA-15, *tris*(4-formyl phenyl)amine loaded silica, A and 2-aminophenol grafted A in the temperature range of 303–1073 K to ascertain the thermal stability of the materials. The results of the studies have been shown in Fig. 7. The good thermal stability of calcined SBA-15 (Fig. 7a) is evident from the curve, with *ca.* 6.5 % weight loss taking place up to 1073 K. This loss is attributed mostly to the loss of adsorbed water and other volatile moieties. This high stability of the silica framework makes it a befitting choice for catalyst supports. The thermal stabilities of the functionalized materials can be determined from their respective TGA plots.⁵⁶ All the samples modified by inserting organic groups show gradual weight-loss in steps depending upon the nature and extent of functionalization. For the 3-APTES, trialdehyde and 2-aminophenol functionalized samples (Fig. 7b-d) the first weight loss of ~ 3-4 % takes place near 373 K due to the removal of physisorbed solvent molecules. For 3-APTES functionalized silica (Fig. 7b) another weight-loss takes place in the range of 530 to 820 K conforming to the removal of the aminopropyl units. The curve for trialdehyde loaded silica, A (Fig. 7c) also follows a similar trend; however, the weight-loss is higher here due to the removal of both aminopropyl and the trialdehyde moieties. The difference corresponds to the amount of trialdehyde that has reacted with the amine group of 3-APTES bound to the mesoporous silica framework. For the 2-aminophenol functionalized silica, the pattern of weight loss remains same due to the removal of different organic counterpart. As anticipated, the weight loss for this sample is higher than A and the difference gives the amount of 2-aminophenol that has been loaded in this step. The extent of functionalization and the amount of organic loading on the silica framework in each material can be determined

from the results. It has been calculated that 0.6590 mmol of 3-APTES is present in 1.0 g of SBA-15 and the amount of trialdehyde loading is 0.1760 mmol/g and that of 2-aminophenol is 0.3680 mmol/g. The amount of copper present in **FMS-Cu(II)** and **FMS-CuO-np** has been ascertained from atomic absorption spectrophotometric study and it has been found that 1.0 g of **FMS-Cu(II)** contains 0.2144 mmol or 13.63 mg of copper and 1.0 g of **FMS-CuO-np** contains 0.2096 mmol or 13.32 mg of copper.

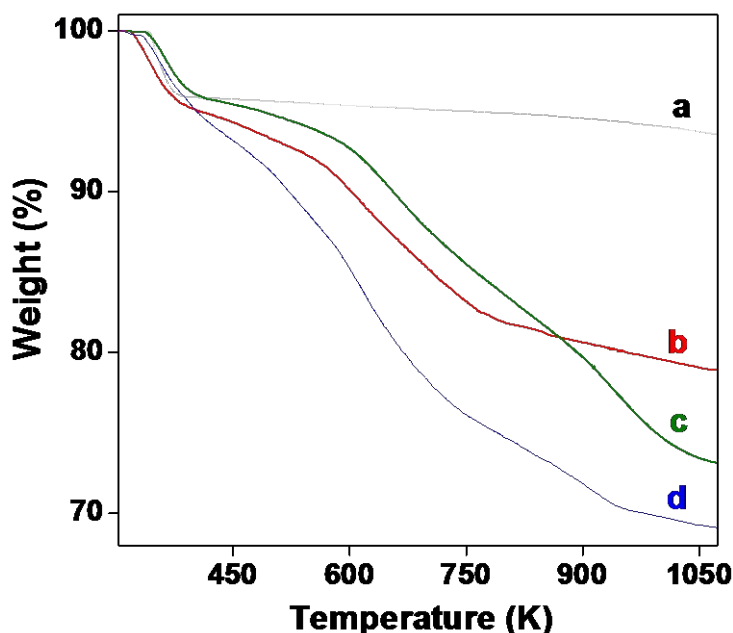


Fig. 7: Thermal analysis data of (a) SBA-15, (b) 3-APTES functionalized SBA-15, (c) trialdehyde functionalized silica (A) and (d) 2-aminophenol functionalized A.

Solid state NMR studies

The chemical environment around a silicon atom can be studied by ^{29}Si MAS NMR spectroscopy. The spectra of the different materials synthesized in this work to obtain **FMS-Cu(II)** and **FMS-CuO-np**, have been illustrated in Fig. 8. For calcined SBA-15, peaks are obtained at -111.51 and -103.38 ppm (Fig. 8a) and these may be attributed to the Q^4 and Q^3 silica centers present in the $\text{Si}(\text{OSi})_n(\text{OH})_{4-n}$ units. Peaks at these positions remain unchanged for the 3-APTES functionalized SBA-15 (Fig. 8b) along with the appearance of two new peaks at -68.07 and -58.16 ppm corresponding to the aminopropyl group incorporated in the framework. These additional peaks correspond to the T^3 ($(\text{SiO})_3\text{Si-R-Si}(\text{OSi})_3$) and T^2 ($(\text{HO})_2(\text{OSi})\text{Si-R-Si}(\text{OSi})_2(\text{OH})$) species,^{57,58} respectively, of the aminopropyl units. The spectra for *tris*(4-formyl phenyl)amine loaded silica, **A**, and 2-aminophenol grafted **A** (Fig. 8c and d) are almost similar to the spectrum obtained for the 3-APTES functionalized silica. This indicates that the chemical environment around silicon centers remains more or less unchanged. For **FMS-Cu(II)**

and **FMS-CuO-np** (Fig. 8e and f, respectively) also the nature of the spectra remain almost similar but in both cases a slight shift in the peak position is observed. Since the imine bonds are present in both the samples the spectra remain intact; the minor shifting of the peak positions arises due to the interaction of the N and O groups present in the functionalized silica with the metal atom/metal oxide nanoparticles through covalent/non-covalent interactions.^{59,60}

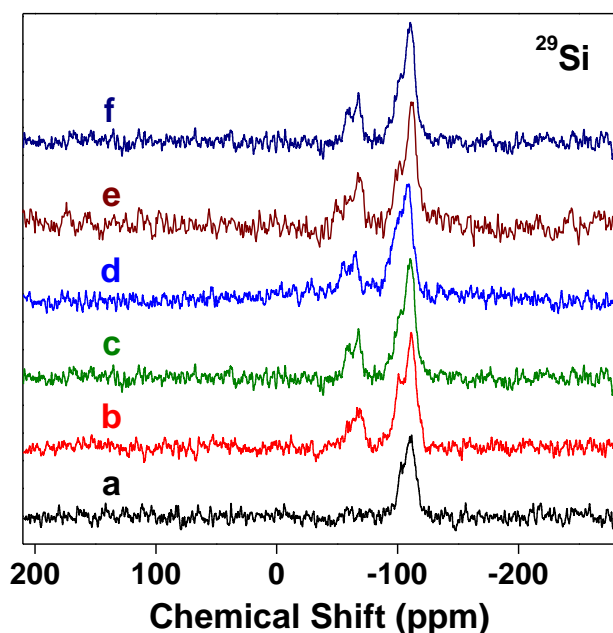


Fig. 8: Solid state ^{29}Si MAS NMR spectra of (a) SBA-15, (b) 3-APTES functionalized SBA-15, (c) trialdehyde functionalized silica (**A**), (d) 2-aminophenol functionalized **A**, (e) **FMS-Cu(II)** and (f) **FMS-CuO-np**.

^{13}C CP (Cross-Polarization) MAS NMR spectra have been recorded for all the materials except calcined SBA-15, which has no carbon containing organic counter-part, and the results are given in Fig. 9. 3-APTES functionalized SBA-15 (Fig. 9a) exhibits peaks at 9.61, 21.73 and 42.65 ppm. The peak at 42.65 ppm arises from the carbon atom next to the amino group. The peaks at 21.73 and 9.61 ppm arise from other two carbon atoms of the propyl chain.⁵⁰ For *tris*(4-formyl phenyl)amine loaded silica, **A** (Fig. 9b), a number of peaks appear in the region of 22.33, 41.95 and 63.50 ppm which correspond to the aliphatic carbon atoms, whereas for the aromatic carbons signals are obtained at 149.91, 164.74 and 129.66 ppm. The presence of imine bond (C=N) and free aldehyde group in **A** can be concluded from their characteristic peaks at 183.31 and 199.82 ppm, respectively. Thus, both the formation of Schiff base from the reaction between the trialdehyde and $-\text{NH}_2$ group of 3-APTES as well as the presence of free aldehyde groups in the material can be confirmed from this spectrum. For 2-aminophenol grafted **A** (Fig. 9c), an additional peak appears in the spectrum at 148.18 ppm due to the inclusion of

phenolic carbon after functionalization with 2-aminophenol. In this material, peaks for free aldehyde groups disappear which confirms the conversion of remaining free $-CHO$ groups of the trialdehyde to $C=N$ after condensation with 2-aminophenol.

For **FMS-Cu(II)** (Fig. 9d), all the peaks corresponding to the aliphatic and aromatic carbons in the previous spectrum appear with marginal chemical shift which confirms retention of the heterogeneous silica support upon complex formation with Cu(II). In case of **FMS-CuO-np** (Fig. 9e), which has been synthesized by the addition of 2-aminophenol and $CuCl_2 \cdot 2H_2O$ in a single step, the peak corresponding to the inclusion of phenolic carbon appears and that for free aldehyde group disappears. The peak corresponding to the imine group from Schiff-base reaction in the consecutive steps is retained. Thus, the nanoparticles which are formed in this reaction are stabilized over the functionalized silica support through non-covalent interaction with the heteroatoms.

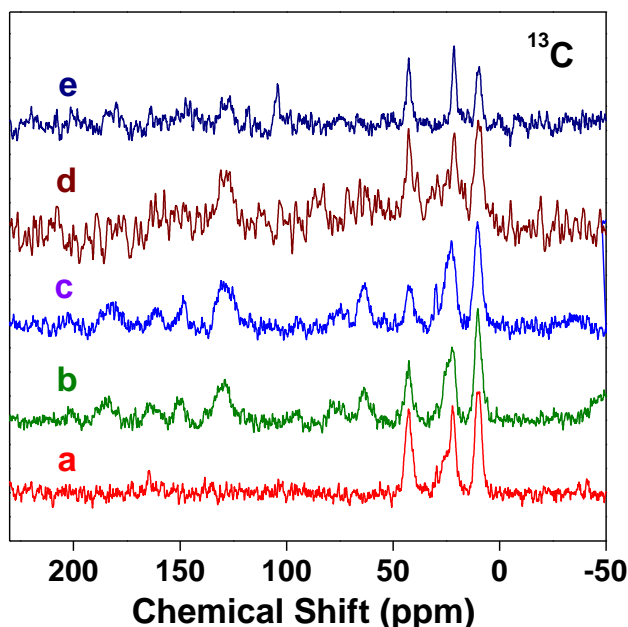


Fig. 9: Solid state ^{13}C CP-MAS NMR spectra (a) 3-APTES functionalized SBA-15, (b) trialdehyde functionalized silica (A), (c) 2-aminophenol functionalized A, (d) **FMS-Cu(II)** and (e) **FMS-CuO-np**.

Catalytic studies

The catalytic efficiency of **FMS-Cu(II)** in which Cu(II) is covalently bound to the functionalized silica support and **FMS-CuO-np** where CuO nanoparticles are dispersed over the same support has been studied for oxidation of some olefins (styrene, α -methyl styrene, cyclohexene, *trans*-stilbene and cyclooctene) in the presence of *tert*-butyl hydroperoxide as the terminal oxidant. The reactions have been performed under identical conditions for both the catalysts, in acetonitrile medium and mild conditions. The conversions have been monitored by gas chromatography and the products have been identified by comparison with known standards as well as GC-MS studies. It has been found that for **FMS-CuO-np** conversion up to 96.5 % is attained within 12 h of the reaction. Thus, the reaction time has been standardized at 12 h for all the catalytic cycles. The total conversions for each substrate with respect to time, from 2 h to 12 h, have been plotted in Fig. 10. After that, the catalytic efficiencies of the two materials that are obtained by minor alteration of the synthetic procedure but giving rise to significant differences in the yield of the products, have been compared. The detail results obtained from the catalytic studies are shown in Table 2. It is quite evident from the results that, both the catalysts are quite effective for oxidation of the olefins. The conversion of the substrates increases rapidly with every hour and within 12 h of the reactions both the catalysts give reasonable yield of the products. However, the CuO nanoparticle based material, **FMS-CuO-np**, is found to be more efficient in carrying out the catalytic transformations compared to **FMS-Cu(II)** where Cu(II) is covalently bound to the silica framework.

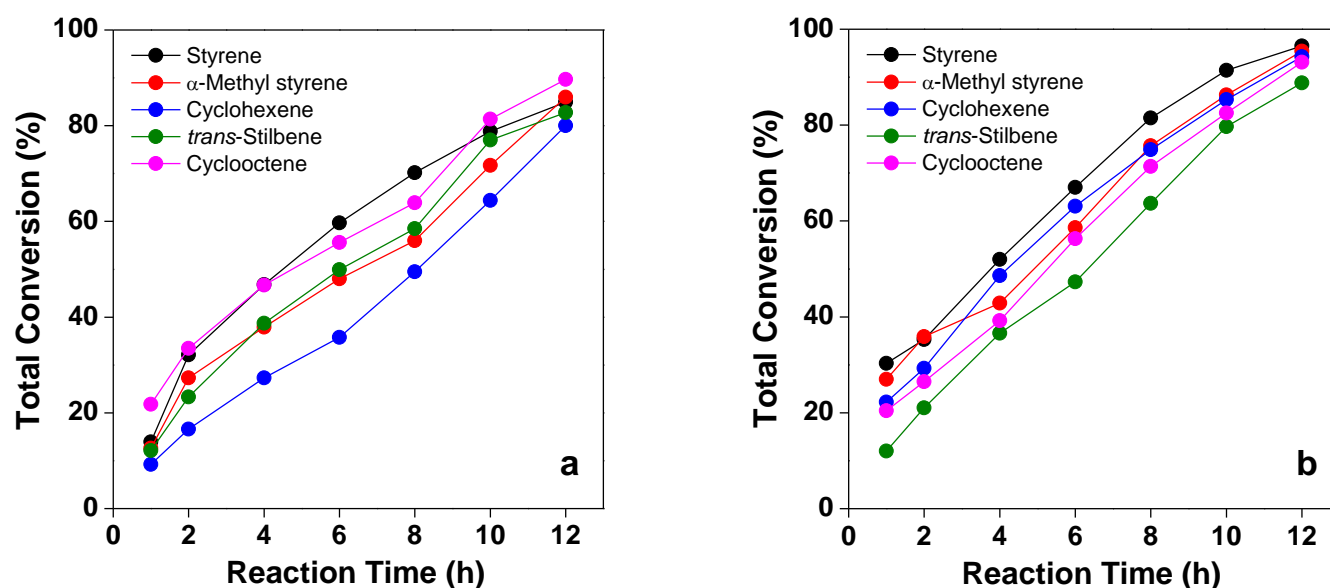
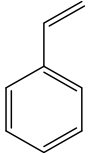
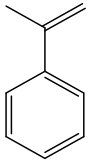
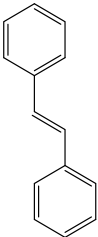


Fig. 10: Oxidation of different substrates in the presence of (a) **FMS-Cu(II)** and (b) **FMS-CuO-np**. Yield of major product from oxidation reaction has been plotted against time

Table 2: Oxidation^a of different olefins in the presence of **FMS-Cu(II)** and **FMS-CuO-np**

Sl. No.	Substrate	Catalyst	Products ^b and Yield (%)			Total Yield (%)	Major Product and Selectivity (%)	TOF ^c
1.			Benzaldehyde	Benzoic acid	Phenylacetaldehyde		Benzaldehyde	
		FMS-Cu(II)	72.20	8.37	4.34	84.91	85.00	33.47
		FMS-CuO-np	83.46	8.48	4.57	96.51	86.47	38.37
		Blank	3.75	2.34	0.51	7.00	53.57	-
2.			α -Methyl styrene oxide	Acetophenone			α -Methyl styrene oxide	
		FMS-Cu(II)	75.08	10.87		85.95	87.35	33.88
		FMS-CuO-np	82.18	13.21		95.39	86.15	37.92
		Blank	4.32	1.66		6.00	72.00	-
3.			2-Cyclohexen-1-one	2-Cyclohexen-1-ol	Cyclohexene Oxide		2-Cyclohexen-1-one	
		FMS-Cu(II)	60.17	12.60	7.23	80.00	75.21	31.53
		FMS-CuO-np	80.17	11.12	2.99	94.28	85.00	37.48
		Blank	2.89	1.08	0.90	5.00	57.80	-
4.			<i>trans</i> -Stilbene oxide	Benzil	Benzaldehyde		<i>trans</i> -Stilbene oxide	
		FMS-Cu(II)	61.90	9.23	11.61	82.74	74.81	32.61
		FMS-CuO-np	66.73	9.71	12.34	88.78	75.16	35.30
		Blank	2.97	1.23	1.85	6.00	49.50	-
5.			Cyclooctene oxide	2-cyclooctene-1-ol	2-cyclooctene-1-one		Cyclooctene oxide	
		FMS-Cu(II)	73.80	9.40	6.50	89.70	82.27	35.36
		FMS-CuO-np	79.10	10.23	3.80	93.13	84.90	37.03
		Blank	2.23	1.28	0.51	4.00	55.75	-

^aSolvent: acetonitrile; temperature: 338 K; oxidant: *tert*-butylhydroperoxide peroxide (TBHP); catalyst: **FMS-Cu(II)** and **FMS-CuO-np**

^bYields are measured after 12 h of the reaction

^cTOF: turnover frequency = moles of substrate converted per mole of metal center per hour

For monitoring the progress of the reactions, aliquots from catalytic reaction mixtures have been collected at regular time intervals and analyzed by gas chromatography. From the chromatographs the amount of the various species formed at different time intervals have been calculated. For lucidity, the results obtained for all the substrates with respect to yield of all the major and minor products in the oxidation reactions for **FMS-Cu(II)** and **FMS-CuO-np** are given individually in Fig. 11-15.

The highest amount of substrate conversion has been found in case of styrene among all the olefins for both the materials and the conversion is better for **FMS-CuO-np** compared to **FMS-Cu(II)**. It is found that for the oxidation of styrene (Table 2, Entry 1) with **FMS-Cu(II)** and **FMS-CuO-np** almost 85.0 % and 96.5 % conversions could be achieved, respectively, within 12 h of the reactions. In both the cases, benzaldehyde has been identified as the major product with *ca.* 85.0 % and 86.5 % selectivity, respectively. With the increase in reaction time, yield of benzaldehyde gradually increases (Fig. 11), both for the catalysts. Apart from benzaldehyde, phenylacetaldehyde and benzoic acid are the other products which are formed in minor amounts.

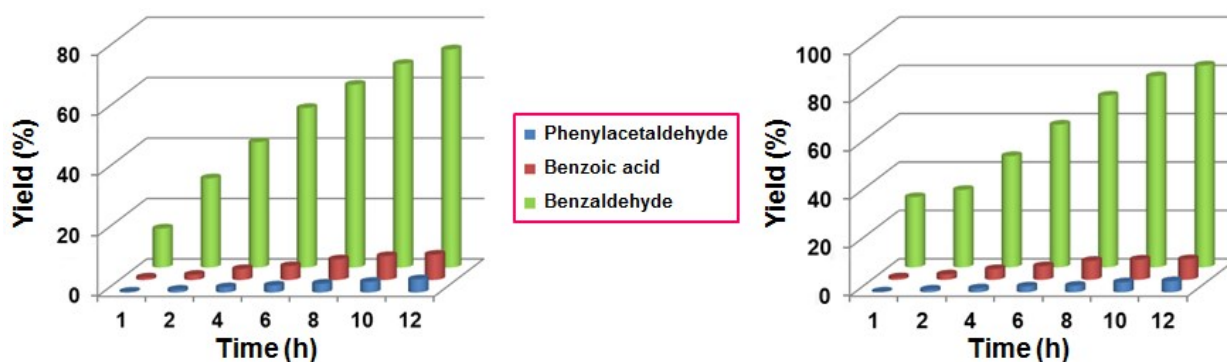


Fig. 11: Oxidation of styrene in the presence of **FMS-Cu(II)** and **FMS-CuO-np**

For the oxidation of α -methyl styrene in presence of TBHP (Table 2, Entry 2), almost 86.0 % and 95.4 % conversions could be achieved for **FMS-Cu(II)** and **FMS-CuO-np**, respectively. The corresponding oxide, α -methyl styrene oxide and acetophenone are found to be the products formed in this oxidation reaction for both the catalysts. The progress of formation of both the products is shown in Fig. 12. Within an hour of the reaction almost 12.0 % and 25.0 % of α -methyl styrene oxide is formed for **FMS-Cu(II)** and **FMS-CuO-np**, respectively. However, after 12 h the formation of the oxide becomes 75.1 % and 82.2 %. Thus, in both the cases, α -methyl styrene oxide has been found to be major product with respective selectivity of *ca.* 87.4 % and 86.2 %. Acetophenone is produced as the minor product in this reaction.

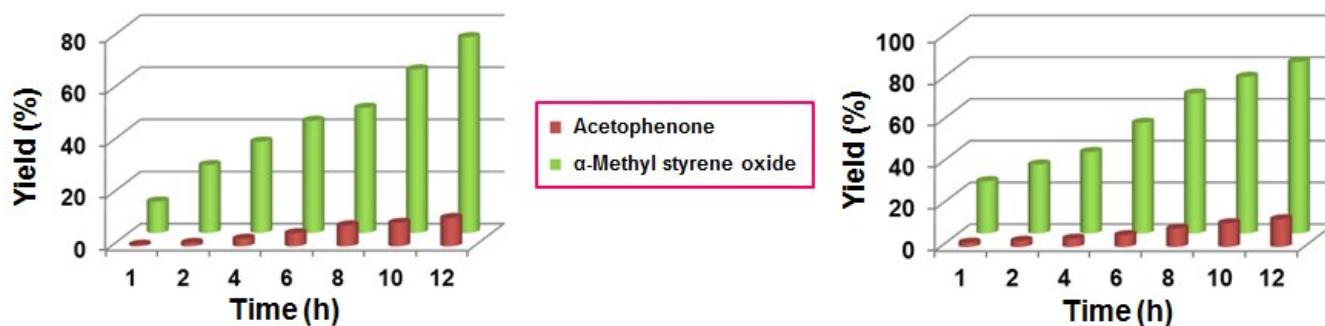


Fig. 12: Oxidation of α -methyl styrene in the presence of **FMS-Cu(II)** and **FMS-CuO-np**

For cyclohexene oxidation (Table 2, Entry 3), almost 80.0 % and 94.3 % conversions have been obtained for **FMS-Cu(II)** and **FMS-CuO-np**, respectively. In this case, three products, namely, 2-cyclohexen-1-one, 2-cyclohexen-1-ol and cyclohexene oxide are formed. 2-cyclohexen-1-one is obtained as the major product and 2-cyclohexen-1-ol and cyclohexene oxide are the other minor products for both the catalysts. After 1 h of the reaction, the amount of 2-cyclohexen-1-one formed is 8 % and 20 %, but within 12 h the conversion reaches to *ca.* 60.2 % and 80.2 % in presence of **FMS-Cu(II)** and **FMS-CuO-np**, respectively (Fig. 13). The selectivity of this product is quite high, *ca.* 75.2 % and 85.0 %, respectively. The increase in the amount of the minor products with the reaction time is also demonstrated in Fig. 13 and it is evident from the figure that the formation of these products increases in the first few hours and then remains almost unaltered.

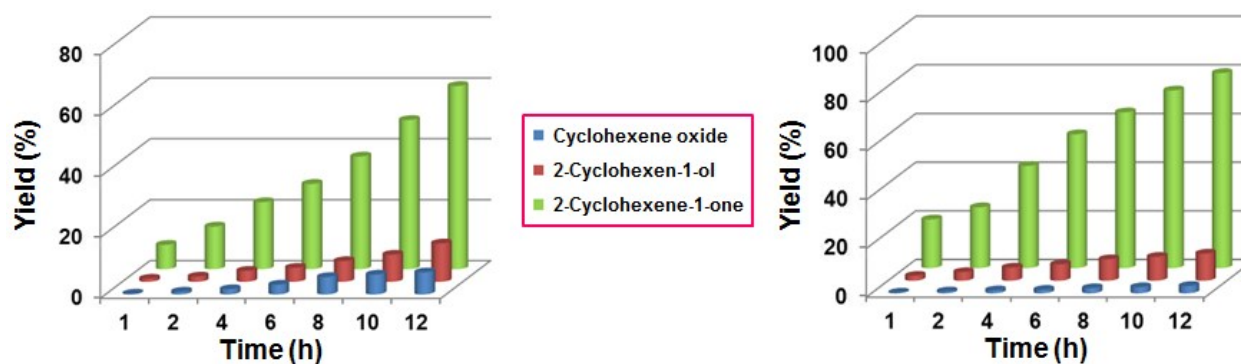


Fig. 13: Oxidation of cyclohexene in the presence of **FMS-Cu(II)** and **FMS-CuO-np**

In case of oxidation of *trans*-stilbene (Table 2, Entry 4), the total conversions for **FMS-Cu(II)** and **FMS-CuO-np** are *ca.* 82.7 % and 88.8 %, respectively. The progress of formation of the major and minor products in this reaction has been shown in Fig. 14. Here *trans*-stilbene oxide has been obtained as the major product and its yield increases from 10.0 % to 61.9 % in the presence of **FMS-Cu(II)** within 1 h to 12 h. For the same reaction,

when CuO nanoparticle based material, **FMS-CuO-np**, is used the increase in yield of the oxide is from 9.0 % to 66.7 % within the same time interval. The selectivity of the product is about 74.8 % and 75.2 %, respectively, for the two catalysts. Benzil and benzaldehyde have been identified as the other minor products of this reaction.

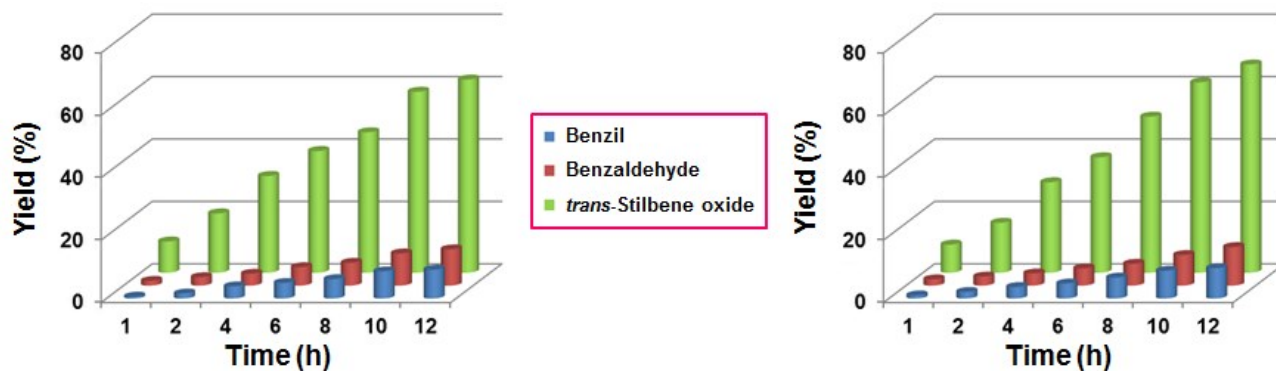


Fig. 14: Oxidation of *trans*-stilbene in the presence of **FMS-Cu(II)** and **FMS-CuO-np**

For the oxidation of cyclooctene, overall conversion of 89.7 % and 93.1 % could be achieved (Table 2, Entry 5) in the presence of **FMS-Cu(II)** and **FMS-CuO-np** as the catalyst. In this case, cyclooctene oxide, 2-cyclooctene-1-ol and 2-cyclooctene-1-one are found to be the different products. The increase in yield of all the products with reaction time has been plotted in Fig. 15. Among them cyclooctene oxide is the major product with 82.3 % and 84.9 % selectivity for **FMS-Cu(II)** and **FMS-CuO-np**, respectively, and 2-cyclooctene-1-ol and 2-cyclooctene-1-one are the minor products. Within 1 h the former catalyzes 20.0 % cyclooctene oxide formation and in 12 h it reaches 73.8 %. For the latter, the increase in the yield of the oxide studied after same time duration is 18.0 % to 79.1 %.

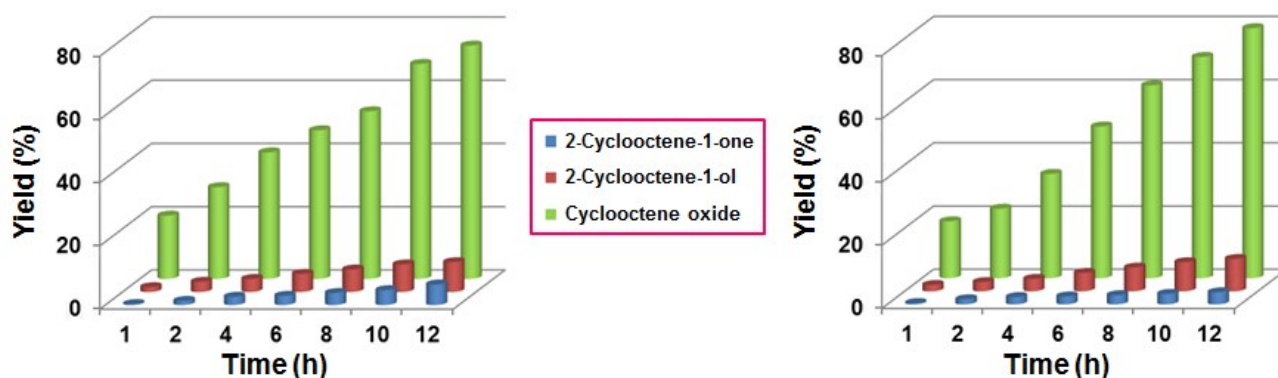


Fig. 15: Oxidation of cyclooctene in the presence of **FMS-Cu(II)** and **FMS-CuO-np**

Thus, the results show that both **FMS-Cu(II)** and **FMS-CuO-np** have excellent catalytic efficiency in these oxidation reactions with high TOF values but the results for **FMS-CuO-np** are superior in every case. **FMS-CuO-np** shows higher TOF values than **FMS-Cu(II)** in each reaction. This may be attributed to the presence of nanoparticles in the former which augments more reactivity than any other conventional metal catalysts through greater surface exposure due to high surface to volume ratio. So more active sites are exposed in **FMS-CuO-np** to catalyze the reaction and thus it exhibits higher product yields with better atom economy. A blank reaction has also been carried out with all the substrates under the same reaction conditions (Table 2) but in the absence of any catalyst. From the small percentage of yield that is obtained for all the blank reactions, it can be concluded that the materials play a pivotal role in the catalytic oxidation of olefins in presence of *tert*-butylhydroperoxide peroxide (TBHP) as the oxidant.

Hot filtration test

To investigate the role of the catalysts and the fact that **FMS-Cu(II)** and **FMS-CuO-np** are responsible for the high conversions in the oxidation reactions, hot filtration tests have been carried out and the results have been illustrated in Fig.16. It is known that for a heterogeneous catalyst presence of unbound metal in the reaction mixture that may catalyze the reaction is not desirable. Thus, to ascertain the heterogeneous nature of a catalyst it should be known that whether metal leaching is taking place from the catalyst framework or any other metal containing species is forming in solution or not. To understand this aspect, hot filtration tests have been performed on styrene oxidation reaction, as a representative case, in the presence of **FMS-Cu(II)** and **FMS-CuO-np**. The catalysts have been separated from the reaction mixture of the respective cycles by filtration under hot condition after 2 hours. Within this time the amount of conversion of styrene has been estimated to be around 32.0 % and 35.0 % in presence of **FMS-Cu(II)** and **FMS-CuO-np**, respectively. After the catalysts have been separated, the reactions are continued with the filtrate containing the substrate, products and TBHP for the usual time duration. It is observed that conversion of styrene proceeds only marginally after this. But in presence of the catalysts, the reactions proceed uninhibited and conversion of styrene increases in regular manner. The slight increase in the conversion of styrene which is observed in absence of the catalysts is attributed to the presence of TBHP oxidant in the mixture. It is also evident from the blank reactions (Table 2) where TBHP is found to oxidize styrene to a small extent. Absence of metal leaching into the reaction medium has been ensured from AAS analysis. After separating the catalysts from the reaction mixtures under hot condition, the filtrates are collected and analyzed by an atomic absorption spectrometer to check whether copper is present in the solutions or not. The results confirmed the absence of any detectable amount of copper in both the reaction mixtures which implied no metal leaching in the solutions from the framework of the solid catalysts.

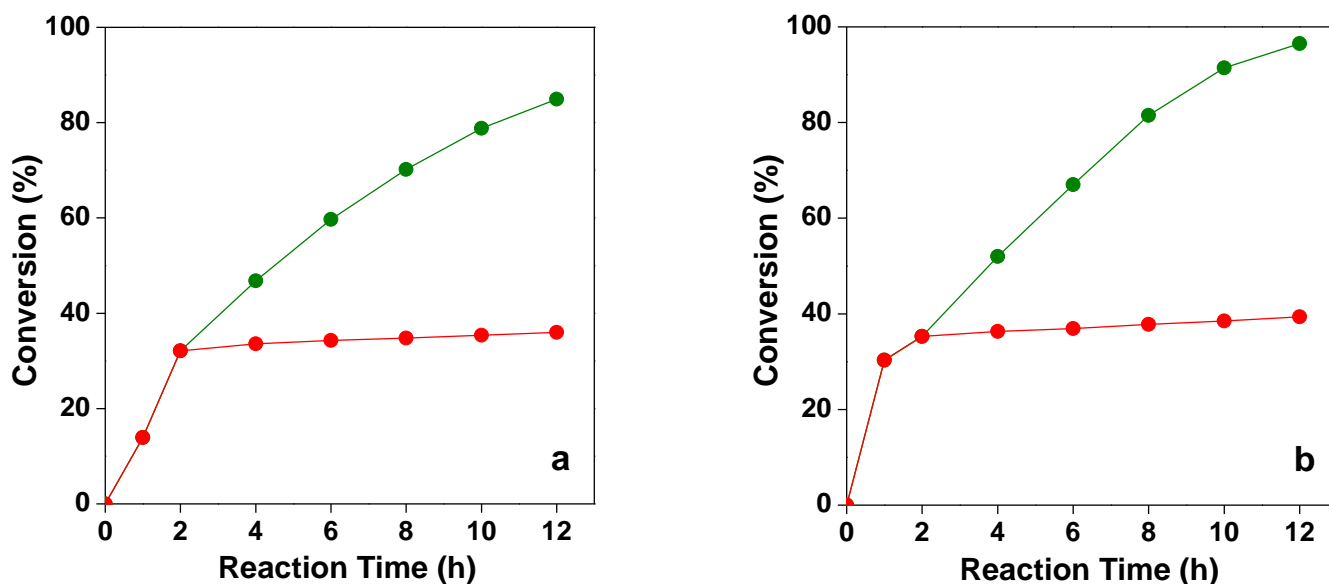


Fig. 16: Hot filtration test for oxidation of styrene in the presence of (a) **FMS-Cu(II)** and (b) **FMS-CuO-np**. Green line/symbol: Uninterrupted reaction in the presence of catalysts. Red line/symbol: Reaction accompanied by hot filtration after 2 h and continued in absence of catalysts.

Recyclability

The most important aspect of a heterogeneous catalyst is its recyclability and to check the reusability of **FMS-Cu(II)** and **FMS-CuO-np** in olefin oxidation reaction, styrene oxidation reaction has been carried out with the recycled catalysts for five times under the optimized condition. In each cycle, 1 mmol of styrene is added to 5 mL of acetonitrile (solvent), 1 mmol of TBHP and the reaction is carried out at 338 K for 12 h. Then the catalyst is recovered from the reaction medium, regenerated by washing and drying and reused in the subsequent catalytic reaction of styrene. The conversion (%) against the number of reaction cycles has been plotted in Fig. 17. For **FMS-Cu(II)**, the conversions in the five consecutive cycles are *ca.* 85 %, 83 %, 79 %, 73.5 %, 70 %, respectively, whereas for **FMS-CuO-np** the same values are *ca.* 96.5 %, 95.5 %, 92 %, 87.5 %, 82 %, respectively. It can be seen from the data that the efficiency of the catalysts remain almost same in the first two cycles, particularly for **FMS-CuO-np**. Overall, there is a gradual decrease in the percentage of conversion in each step up to the fifth cycle. The reason behind the steady drop in conversion may be attributed to somewhat loss in porosity of the catalysts and their porous structure due to exposure in reaction medium in presence of solvent and oxidant for a prolonged period. Small decrease in surface area of the recovered catalysts has been witnessed from the nitrogen adsorption/desorption studies. However, from the considerably high conversion amount in the fifth cycle, particularly so for **FMS-CuO-np** (82.0 %), it can be concluded that the catalysts have good recyclability.

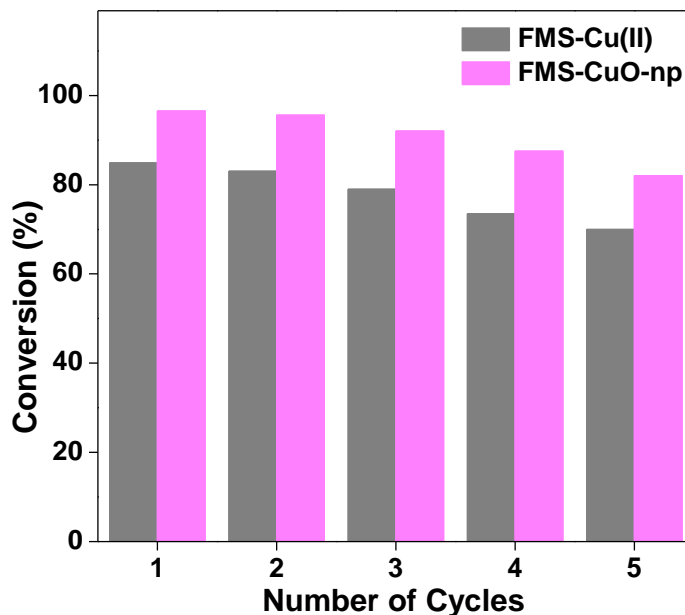


Fig. 17: Recycling efficiency of **FMS-Cu(II)** and **FMS-CuO-np** in oxidation of styrene

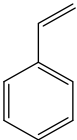
The catalytic oxidation of styrene in presence of TBHP has also been carried out in different solvents to examine solvent dependence and subsequently choose the suitable medium. The solvents include water, methanol, dichloromethane, toluene and acetonitrile and the conversions obtained in the reactions have been given in Table 3. It is evident from the results that the highest yield is obtained when acetonitrile is used as the solvent and hence it has been used in all the catalytic reactions studied in this work. Apart from that, acetonitrile stabilizes Cu(I) species formed in solution by coordinating with the metal center.⁶¹ The Cu(I) species that is formed as an intermediate during the catalytic cycle is also responsible for the performance of the Cu-based materials as efficient catalysts in the oxidation reactions.

Table 3: Oxidation of styrene in presence of **FMS-Cu(II)** and **FMS-CuO-np** in different solvents

Sl. No.	Reaction medium	Yield (%)	
		FMS-Cu(II)	FMS-CuO-np
1.	Water	18	23
2.	Methanol	28	36
3.	Dichloromethane	26	49
4.	Toluene	43	54
5.	Acetonitrile	85	97

The catalytic oxidation of styrene as a representative case has been studied in the presence of TBHP at different temperatures in order to understand the effect of temperature on the reactions. The reactions have been carried out for 12 h and the results are given in Table 4. The reactions performed at ambient condition, the temperature being measured as 303 K for that particular day, showed quite low yields with both the catalysts (Entries 1 and 6). With gradual increase in temperature to 318 K (Entries 2 and 7), 328 K (Entries 3 and 8), 338 K (Entries 4 and 9) and 348 K (Entries 5 and 10), it is observed that the conversion of the substrates to the products gradually increases. However, if the reaction yields are compared at 338 K and 348 K for **FMS-Cu(II)** (Entries 4 and 5) and **FMS-CuO-np** (Entries 9 and 10), it is found that only marginal increase in the conversion takes place on such increase of temperature. On the other hand, the increase in yields when the temperature is increased from 328 K to 338 K is considerably high (Entries 3 and 4 for **FMS-Cu(II)** and Entries 8 and 9 for **FMS-CuO-np**). Thus, the temperatures for all the reactions in the study have been optimized at 338 K.

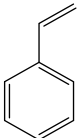
Table 4: Oxidation of styrene in presence of **FMS-Cu(II)** and **FMS-CuO-np** at different temperatures

Sl. No.	Substrate	Temperature (K)	Catalyst	Products ^b and Yield (%)			Total Yield (%)
				Benzaldehyde	Benzoic acid	Phenylacetaldehyde	
							
1.		303*	FMS-Cu(II)	23.99	11.75	0.00	35.74
2.		318	FMS-Cu(II)	29.54	15.29	1.75	46.58
3.		328	FMS-Cu(II)	45.89	8.35	2.40	56.64
4.		338	FMS-Cu(II)	72.20	8.37	4.34	84.91
5.		348	FMS-Cu(II)	73.55	8.43	4.38	86.36
6.		303*	FMS-CuO-np	26.18	15.74	0.00	41.92
7.		318	FMS-CuO-np	31.26	15.67	1.68	48.61
8.		328	FMS-CuO-np	52.48	8.16	2.94	63.58
9.		338	FMS-CuO-np	83.46	8.48	4.57	96.51
10.	348	FMS-CuO-np	84.08	8.97	4.62	97.67	

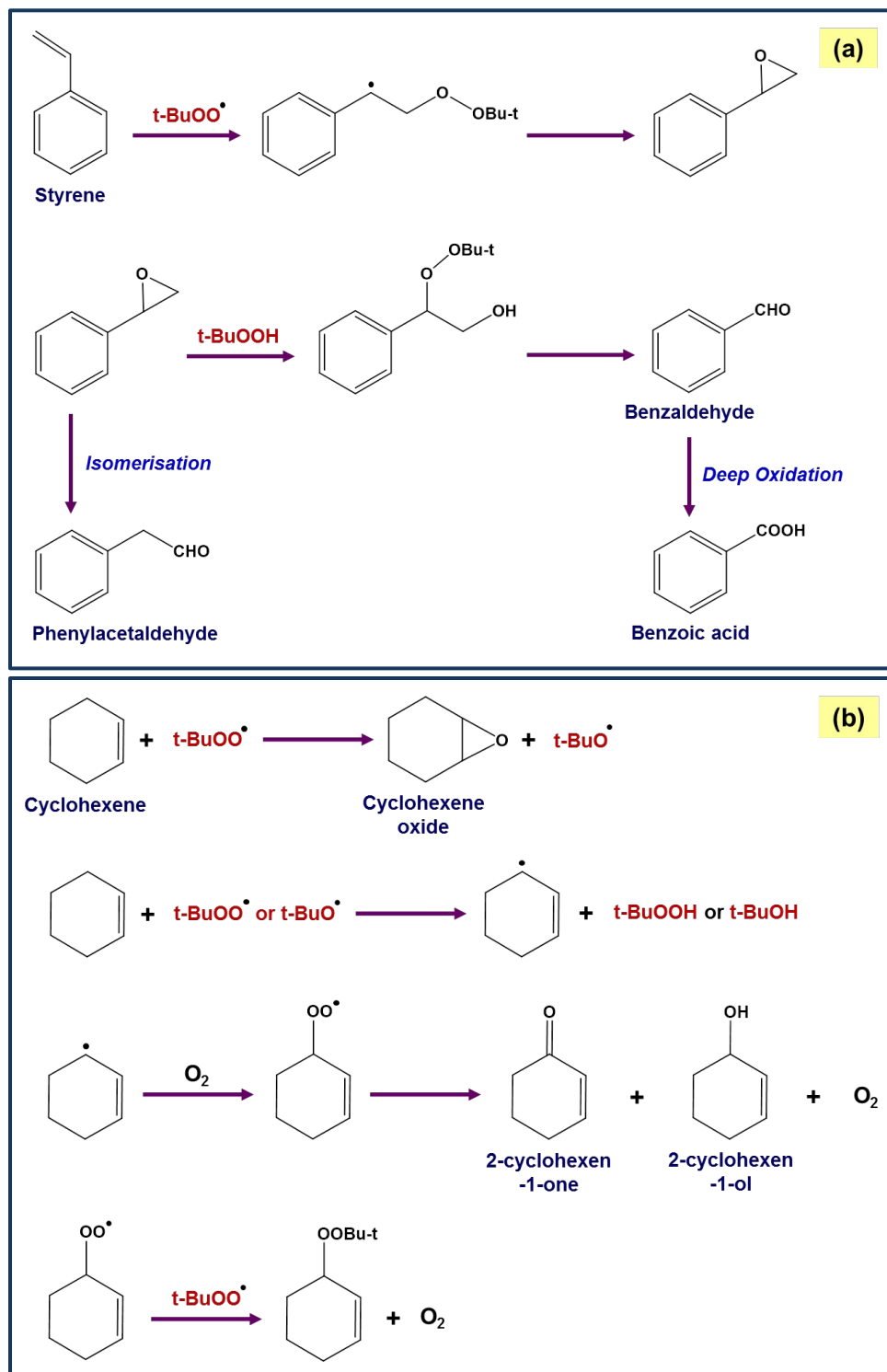
*Ambient temperature was recorded for the day of the experiment as 303 K

To check the efficiency of other oxidizing agent in the catalytic reactions, styrene oxidation reactions have been carried out in presence of H₂O₂ and O₂ instead of TBHP keeping the other conditions same. The comparative results, when TBHP, H₂O₂ and O₂ are used as oxidants, have been given in Table 5. In presence of both the catalysts poor yields are obtained with H₂O₂ (Entries 2 and 5) compared to TBHP (Entries 1 and 4). On the other hand, in presence of O₂ almost no/insignificant conversion takes place (Entries 3 and 6) in presence of any of the catalyst. Hence, TBHP has been chosen as the oxidant to carry out all the oxidation reactions.

Table 5: Oxidation of styrene in presence of **FMS-Cu(II)** and **FMS-CuO-np** using TBHP and H₂O₂

Sl. No.	Substrate	Oxidant	Catalyst	Products ^b and Yield (%)			Total Yield (%)
				Benzaldehyde	Benzoic acid	Phenylacetaldehyde	
1.		TBHP	FMS-Cu(II)	72.20	8.37	4.34	84.91
2.		H ₂ O ₂	FMS-Cu(II)	62.46	3.84	2.54	68.84
3.		O ₂	FMS-Cu(II)	0.00	0.00	0.00	0.00
4.		TBHP	FMS-CuO-np	83.46	8.48	4.57	96.51
5.		H ₂ O ₂	FMS-CuO-np	68.23	4.06	4.46	76.75
6.		O ₂	FMS-CuO-np	1.85	0.00	0.00	1.85

Mechanism



Scheme 2: Plausible mechanistic route for oxidation of olefins: (a) Styrene and (b) Cyclohexene

To explain the catalytic oxidation of olefins by the Cu(II) containing samples, **FMS-Cu(II)** and **FMS-CuO-np**, plausible mechanisms (Scheme 2) have been proposed based on the previously reported literature. It is well-established that the overall reaction proceeds through a radical mechanism where $t\text{BuOO}^\bullet$ and $t\text{BuO}^\bullet$ are the radicals which are formed by the reaction between TBHP and Cu(II). Cu(II) gets reduced to Cu(I)⁶²⁻⁶⁵ with subsequent formation of the radical species. The various steps involved in the oxidation of styrene and cyclohexene, as representative cases, through radical mechanism have been depicted in the scheme.⁶⁶⁻⁶⁸ Other olefins are expected to go through similar reaction pathways. The probable reason behind the formation of different major and minor products in these reactions is the competition between oxidation of the C=C bond and the allylic bond. In case of styrene, there is no allylic double bond and thus it forms the corresponding epoxide first on oxidation of the double bond. Then benzaldehyde is formed by ring opening of the styrene epoxide. On the other hand, cyclohexene first produces the corresponding epoxide on oxidation of the double bond⁶⁹ which can then undergo allylic oxidation resulting in the formation of 2-cyclohexen-1-one as the major product.

Conclusions

In this work, two different materials, namely, **FMS-Cu(II)** and **FMS-CuO-np**, have been synthesized based on functionalized mesoporous SBA-15 silica framework by a simple change in the sequence of addition of the reagents. In **FMS-Cu(II)**, copper is in +II oxidation state and anchored with 2-aminophenol grafted *tris*(4-formyl phenyl) amine SBA-15 by covalent bond and in **FMS-CuO-np**, CuO nanoparticles are immobilized over the same functionalized silica matrix. The generation of CuO nanoparticles takes place *in situ* in the presence of 2-aminophenol which also acts as a stabilizer for the metal oxide nanoparticles. The materials have been characterized thoroughly to establish the various aspects of their structure. Both the materials have reasonable surface area to act as promising heterogeneous catalyst and thus they have been tested for olefin oxidation reaction as a representative case. Both the materials show excellent conversion and selectivity in the oxidation reaction of a number of olefin compounds; the rate of conversion being highest for styrene among all the substrates for both the catalysts. Different products are obtained through epoxidation and oxidation at allylic site of the olefins with progress of the reactions. Both **FMS-Cu(II)** and **FMS-CuO-np** are found to be recyclable and their activity is retained significantly for several cycles and the materials can be reused at least to the extent of five consecutive reaction cycles. However, due to the specific advantages of the properties of nanoparticles, particularly their high surface to volume ratio **FMS-CuO-np** is found to be more efficient compared to **FMS-Cu(II)**. The basic idea of this work is the syntheses of two different materials, one with covalently bound Cu(II) and other with CuO nanoparticles, using a method which is apparently not related to the main reaction but produces a substantial impact on the structure of the materials and becomes the parameter which quite well defines their catalyst characteristics.

comparative study of the catalytic performance between. And the results point to the fact that presence of nanoparticles certainly enhances the catalytic properties.

Acknowledgements

MN acknowledges financial support from DST-SERB (SB/FT/CS-004/2014 dated 27/06/2014), India and WB-DST, India (ST/P/S&T/15G-20/2018). Authors are thankful to Hiroshi Uyama of Osaka University for solid state NMR studies, Partha Roy of Jadavpur University for providing GC and GC-MS facilities, Narayan Pradhan of Indian Association for the Cultivation of Science for providing TEM facility and G Ghosh of Visva-Bharati for AAS studies.

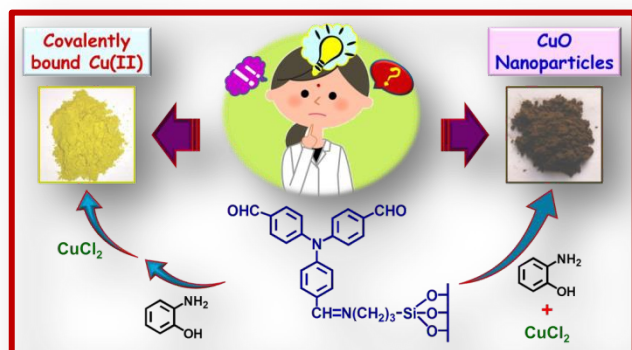
References

1. P. Drabina, J. Svoboda and M. Sedlák, *Molecules*, 2017, **22**, 1.
2. N. Scotti, N. Ravasio, R. Psaro, C. Evangelisti, S. Dworakowska, D. Bogdal and F. Zaccheria, *Catal. Commun.*, 2015, **64**, 80.
3. D. Astruc, F. Jaime and R. Aranzaes, *Angew. Chem. Int. Ed.*, 2005, **44**, 7852.
4. X. Cui, W. Li, P. Ryabchuk, K. Junge and M. Beller, *Nature Catalysis*, 2018, **1**, 385.
5. L. C. Lee, J. He, J. Q. Yu and C. W. Jones, *ACS Catal.*, 2016, **6**, 5245.
6. M. Nandi and H. Uyama, *RSC Adv.*, 2014, **4**, 20847.
7. J. Čejka, R. E. Morris and D. P. Serrano, *Catal. Sci. Technol.*, 2016, **6**, 2465.
8. L. Shang, T. Bian, B. Zhang, D. Zhang, L.-Z. Wu, C.-H. Tung, Y. Yin and T. Zhang, *Angew. Chem., Int. Ed.*, 2014, **53**, 250.
9. M.-R. Gao, X. Cao, Q. Gao, Y.-F. Xu, Y.-R. Zheng, J. Jiang and S.-H. Yu, *ACS Nano*, 2014, **8**, 3970.
10. X. Xu, Y. Li, Y. Gong, P. Zhang, H. Li and Y. Wang, *J. Am. Chem. Soc.*, 2012, **134**, 16987.
11. H. Noh, Y. Cui, A. W. Peters, D. R. Pahls, M. A. Ortuñ, N. A. Vermeulen, C. J. Cramer, L. Gagliardi, J. T. Hupp and O. K. Farha, *J. Am. Chem. Soc.*, 2016, **138**, 14720.
12. H. S. Oh, H. N. Nong, T. Reier, A. Bergmann, M. Gliech, J. F. D. Araújo, E. Willinger, R. Schlögl, D. Teschner and P. Strasser, *J. Am. Chem. Soc.*, 2016, **138**, 12552.
13. C. M. A. Parlett, K. Wilson and A. F. Lee, *Chem. Soc. Rev.*, 2013, **42**, 3876.
14. L. Yin and J. Liebscher, *Chem. Rev.*, 2007, **107**, 133.
15. C. T. Kresge, M. E. Leonowicz, W. J. Roth, J. C. Vartuli and J. S. Beck, *Nature*, 1992, **359**, 710.
16. M. Nandi, P. Roy, H. Uyama and A. Bhaumik, *Dalton Trans.*, 2011, **40**, 12510.
17. T. Das, R. Chatterjee, A. Majee, H. Uyama, D. Morgan and M. Nandi, *Dalton Trans.*, 2019, **48**, 17874.
18. I. O-Jiménez, N. G. Bastús and V. Puentes, *J. Phys. Chem. C*, 2011, **115**, 15752.
19. Z. Zhao, Y. Coppel, J. Fitremann, P. Fau, C. Roux, C. Lepetit, P. Lecante, J.-D. Marty, C. Mingotaud and M. L. Kahn, *Chem. Mater.*, 2018, **30**, 8959.
20. A.S. Danial, M. I. Awad, F. A. Al-Odail and M.M. Saleh, *J. Mol. Liq.*, 2017, **225**, 919.
21. N. Liakakos, B. Cormary, X. Li, P. Lecante, M. Respaud, L. Maron, A. Falqui, A. Genovese, L. Vendier, S. Koinis, B. Chaudret, and K. Soulantica, *J. Am. Chem. Soc.*, 2012, **134**, 17922.
22. T. Das, H. Uyama and M. Nandi, *New J. Chem.*, 2018, **42**, 6416.
23. T. Das, H. Uyama and M. Nandi, *J. Solid State Chem.*, 2018, **260**, 132.
24. C. Xu, X. Wang, J. Zhu, X. Yang and L. Lu, *J. Mater. Chem.*, 2008, **18**, 5625.
25. X. Zhou, W. Xu, G. Liu, D. Panda and P. Chen, *J. Am. Chem. Soc.*, 2010, **132**, 138.
26. D. Chakraborty, S. Nandi, D. Mullangi, S. Haldar, C. P. Vinod and R. Vaidhyanathan, *ACS Appl. Mater. Interfaces*, 2019, **11**, 15670.

27. S. Wang, Z. Wang and Z. Zha, *Dalton Trans.*, 2009, 9363.
28. M. B. Thathagar, J. Beckers and G. Rothenberg, *J. Am. Chem. Soc.*, 2002, **124**, 11858.
29. T. Kamal, *Polymer Testing*, 2019, **77**, 105896.
30. L. Xu, J. Zhang, Z. Li, Q. Ma, Y. Wang, F. Cui and T. Cui, *New J. Chem.*, 2019, **43**, 520.
31. X. Xiong, C. You, Z. Liu, A. M. Asiri and X. Sun, *ACS Sustainable Chem. Eng.*, 2018, **6**, 2883.
32. M. Ouchi, T. Terashima and M. Sawamoto, *Chem. Rev.*, 2009, **109**, 4963.
33. Q. Wang, Y. Su, L. Li and H. Huang, *Chem. Soc. Rev.*, 2016, **45**, 1257.
34. A. Nodzevska, A. Wadolowska and M. Watkinson, *Coord. Chem. Rev.*, 2019, **382**, 181.
35. M. Sankaralingam, M. Balamurugan and M. Palaniandavar, *Coord. Chem. Rev.*, 2020, **403**, 213085.
36. A. Bhattacharjee, S. Halder, K. Ghosh, C. Rizzoli and P. Roy, *New J. Chem.*, 2017, **41**, 5696.
37. C. Deraedt and D. Astruc, *Acc. Chem. Res.*, 2014, **47**, 494.
38. J. H. Xie, S. F. Zhu and Q. L. Zhou, *Chem. Rev.*, 2011, **111**, 1713.
39. F. Wang, S. Yu and X. Li, *Chem. Soc. Rev.*, 2016, **45**, 6462.
40. K. N. Lee and M. Y. Ngai, *Chem. Commun.*, 2017, **53**, 13093.
41. R. D. Chakravarthy, V. Ramkumar and D. K. Chand, *Green Chem.*, 2014, **16**, 2190.
42. J. Q. Bond, D. M. Alonso, D. Wang, R. M. West and J. A. Dumesic, *Science*, 2010, **327**, 1110.
43. X. L. Yang, X. Xing, J. Li, Y. H. Liu, N. Wang and X. Q. Yu, *RSC Adv.*, 2019, **9**, 6003.
44. M. Selvaraj and T. G. Lee, *J. Phys. Chem. B*, 2006, **110**, 21793.
45. D. Ji, R. Zhao, G. Lv, G. Qian, L. Yan, and J. Suo, *Appl. Catal. A Gen.*, 2005, **281**, 39.
46. R. Noyori, M. Aoki and K. Sato, *Chem. Commun.*, 2003, 1977.
47. K. A. Jorgensen, *Chem. Rev.*, 1989, **89**, 431.
48. T. Mukaiyama and T. Yamada, *Bull. Chem. Soc. Jpn.*, 1995, **68**, 17.
49. T. Mallegol, S. Gmouh, M. A. A. Meziane, M. B.-Desce and O. Mongin, *Synthesis*, 2005, **11**, 1771.
50. T. Das, D. Singha, A. Pal and M. Nandi, *Sci. Rep.*, 2019, **9**, 19378.
51. O. Olkhovik and M. Jaroniec, *J. Am. Chem. Soc.*, 2005, **127**, 60.
52. V. V. T. Padil and M. Černík, *Int. J. Nanomed.*, 2013, **8**, 889.
53. A. Stein, *Adv. Mater.*, 2003, **15**, 763.
54. M. Thommes, K. Kaneko, A. V. Neimark, J. P. Olivier, F. Rodriguez-Reinoso, J. Rouquerol and K. S. Sing, *Pure Appl. Chem.*, 2015, **87**, 1051.
55. T. Tanev and T. J. Pinnavaia, *Science*, 1996, **271**, 1267.
56. C. Sarkar, P. Koley, I. Shown, J. Lee, Y.-F. Liao, K. An, J. Tardio, L. Nakka, K. H. Chen and J. Mondal, *ACS Sustainable Chem. Eng.*, 2019, **7**, 10349.
57. S. Inagaki, S. Guan, Y. Fukushima, T. Ohsuna and O. Terasaki, *J. Am. Chem. Soc.*, 1999, **121**, 9611.

58. S. Inagaki, S. Guan, T. Ohsuna and O. Terasaki, *Nature*, 2002, **416**, 304.
59. C. Sarkar, S. Pendem, A. Shrotri, D. Q. Dao, P. P. T. Mai, T. N. Ngoc, D. R. Chandaka, T. V. Rao, Q. T. Trinh, M. P. Sherburne and J. Mondal, *ACS Appl. Mater. Interfaces*, 2019, **11**, 11722.
60. S. C. Shit, R. Singuru, S. Pollastri, B. Joseph, B. S. Rao, N. Lingaiah and J. Mondal, *Catal. Sci. Technol.*, 2018, **8**, 2195.
61. C. L. Gatlin, F. Tureček and T. Valsar, *Anal. Chem.*, 1994, **66**, 3950.
62. J. K. Kochi, *Tetrahedron*, 1962, **18**, 483.
63. J. K. Kochi, *J. Am. Chem. Soc.*, 1962, **84**, 1572.
64. G. Rothenberg, L. Feldberg, H. Wiener and Y. Sasson, *J. Chem. Soc., Perkin Trans.*, 1998, **2**, 2429.
65. U. Junghans, C. Suttikus, J. Lincke, D. Lässig, H. Krauyscheid and R. Gläser, *Micropor. Mesopor. Mater.*, 2015, **216**, 151.
66. L. M. Slaughter, J. P. Collman, T. A. Eberspacher and J. I. Brauman, *Inorg. Chem.*, 2004, **43**, 5198.
67. F. Farzaneh, J. Taghavi, R. Malakooti and M. Ghandi, *J. Mol. Catal. A*, 2006, **244**, 252-257.
68. M. Sarkheil and M. Lashanizadegan, *Appl. Organometal. Chem.*, 2017, **31**, 3726.
69. E. L. Eliel and S. H. Wilen, *Stereochemistry of Organic Compounds*, John Wiley, New York, 1994.

Table of Content



Big effect of a small change: formation of CuO nanoparticles instead of covalently bound Cu(II) over functionalized mesoporous silica and its impact on catalytic efficiency

Trisha Das, Debdas Singha and Mahasweta Nandi

Covalently bound copper(II) and CuO nanoparticles on mesoporous silica have been prepared by changing addition sequence of reagents; latter shows better catalytic activity.